Networks and Heterogeneous Media

https://www.aimspress.com/journal/nhm

NHM, 21(5): 1968–1986.
DOI: 10.3934/nhm.2026074
Received: 11 August 2026
Revised: 11 September 2026
Accepted: 24 September 2026
Published: 08 October 2026

Research Article

Event-triggered cooperative control of networked vehicle platoons under intermittent communication

Xin Wen[1,3], **Tingting Yu**[1,2,3,*] **and Ruibing Li**[1,3]

[1] School of Mathematics and Statistics, Heilongjiang University, Harbin 150080, China
[2] School of Automation, Beijing Institute of Technology, Beijing 100081, China
[3] Heilongjiang Provincial Key Laboratory of the Theory and Computation of Complex Systems, Harbin 150080, China

* **Correspondence:** Email: tingtingyu@hlju.edu.cn; Tel: +8615245080953.

Abstract: This work addresses the consensus tracking problem for connected vehicle systems under time-varying communication topologies and persistent intermittent communication. A coordinated event-triggered protocol relying only on local and neighboring vehicle information is developed to enhance resilience against channel blockages while reducing bandwidth usage and energy consumption. The communication digraph switches within a finite set of directed graphs, each containing a spanning tree rooted at the lead vehicle. By constructing a piecewise Lyapunov functional and applying the average dwell-time technique, sufficient conditions in terms of linear matrix inequalities are derived to guarantee exponential stability and leader-following consensus in the tracking error dynamics. The proposed scheme is proven to exclude Zeno behavior, ensuring a positive lower bound on inter event intervals. Simulation results confirm the effectiveness and superiority of the strategy under simultaneous switching topologies and intermittent communication.

Keywords: connected vehicle systems; switching topologies; intermittent communication; event-triggered control; leader-follower consensus

1. Introduction

Multi–agent coordination control denotes a control methodology whereby a collective of agents, via networked information interchange, achieve cooperative behavior to attain a unified global objective. Given the ubiquity of its application across domains including, but not limited to coordinated vehicle fleet management, synergistic sensor fusion and decision-making, and decentralized traffic control systems, this paradigm continues to motivate extensive research. Extensive research has focused on the intricacies of multi-agent collaborative orchestration. Representative research topics

include encompass collective swarming phenomena [1–3], flocking dynamics [4–6], and formation control strategies [7]. Given the pervasive deployment of networked multi-agent frameworks in operational fields such as unmanned system coordination, collaborative perception, and distributed decision-making, their coordinated control problems have attracted significant attention [8]. As an important application form of multi-agent systems in intelligent transportation frameworks, vehicle platooning accomplishes the concerted regulation of a prescribed inter-vehicle distance and speed. It effectively alleviates traffic congestion, improves road capacity, and reduces energy consumption [9–11]. In networked vehicle systems, consensus control constitutes the foundational framework for achieving collaborative objectives, wherein the system's resilience and cybersecurity performance assume critical significance, particularly under conditions of exogenous disturbances or adversarial intrusions. Nevertheless, within operational vehicular networks, communication topologies are seldom static; rather, they undergo continuous reconfiguration due to relative inter-vehicular motion or dynamic fluctuations in communication linkages. This time-varying network configuration introduces significant complexities in both systemic analysis and the control architecture design.

On the other hand, networked control systems commonly suffer from cybersecurity risks, particularly under intermittent communication conditions. These intrusions block communication channels, leading to interruptions in data exchange among agents and seriously degrading the collective coordination performance and dynamic stability of the system. Hence, a key challenge for connected vehicle control systems lies in achieving consensus amidst adversarial intermittent communication. A great number of research efforts have been devoted to addressing this challenge in existing literature [12–14]. For instance, the distributed secure platoon controllers postulated in [12, 15] were designed to mitigate the adverse effects of intermittent communication, which are conventionally modeled as persistent packet dropouts. Although considerable attention has been paid to the coordinated control of multi-agent systems subject to intermittent communication under fixed topologies, designing effective control strategies to counter intermittent communication under switching topologies remains a challenging research problem.

Furthermore, network bandwidth limitation acts as a fundamental constraint. The conventional time-triggered mechanism adopted in most existing platoon control systems [15–17] performs periodic data transmission regardless of real system operation requirements, thus leading to low utilization of communication resources. In contrast, event-triggered control only triggers communication and control updates when necessary, which greatly reduces the communication frequency and energy consumption, and further improves resource utilization efficiency and the system's security. Accordingly, a variety of event-driven control strategies have been presented in the literature [18–20]. Nevertheless, the design of decentralized event-triggered controllers that can ensure rigorous stability and consensus performance, especially under the coexistence of switching topologies and intermittent communication, has received limited research attention. Recent studies have further advanced event-triggered coordination and resilient control from complementary perspectives. Zhao et al. [21] developed a funnel-based predefined-time output-feedback fuzzy adaptive event-triggered platoon controller for heterogeneous vehicles. Deng et al. [22] investigated event-triggered Nash equilibrium seeking for high-order nonlinear multi-agent systems. Fan et al. [23] studied cooperative resilient nonconvex optimization of nonlinear multi-agent systems under denial-of-service attacks, while Zhang et al. [24] reported robust event-triggered path-following control for a rotor-assisted vehicle with output constraints. These recent results demonstrate the continuing importance of event-triggered

communication, resilience, and resource-efficient coordination, and motivate the present study of their combined treatment in vehicle platoons with switching topologies and intermittent communication. Although the contribution in [25] posited a resilient event-triggered scheme, pivotal challenges persist in concurrently addressing the intricate interplay between sampling intervals and attack duration, and in constructing a comprehensive stability analysis framework subject to these coupled constraints.

Motivated by the discussion above, the paper is devoted to examining the leader–follower concordance problem in networked vehicular systems operating under adversarial intermittent communication and reconfigurable communication topologies. The main contributions of this paper are fourfold.

1. A novel distributed event-triggered control protocol is developed, which only relies on local and neighboring vehicle state information. The controller can adaptively respond to communication topology reconfiguration and maintain operational robustness against intermittent communication by adopting a zero control input strategy.

2. A switched system modeling framework is established to fully characterize the coupling relationship among intermittent communication, event-triggering mechanisms, and dynamic network topologies.

3. By constructing piecewise Lyapunov functionals and using the average dwell-time methodology, sufficient conditions articulated as linear matrix inequalities are derived, ensuring the exponential stabilization of tracking error dynamics and consensus attainment.

4. Zeno behavior is excluded via rigorous mathematical analysis. In addition, a linear matrix inequality (LMI)-based controller gain synthesis is provided, after which the triggering parameter is selected from the admissible interval in Theorem 1. The numerical study is used to assess convergence, communication efficiency, robustness to intermittent communication, and adaptability to topology variations rather than to claim uniform superiority over all comparison cases.

2. Problem formulation

Throughout this paper, $\|z\|$ denotes the Euclidean norm for a vector z, and $\|M\|$ denotes the induced matrix 2-norm for a matrix M.

2.1. Basic graph theory

A team consisted of $N+1$ connected vehicles is considered. A directed graph $\mathcal{G}_{\sigma(t)}$ is a pair $(\mathcal{V}, \mathcal{E}_{\sigma(t)})$, where $\mathcal{V} = \{0, 1, 2, \ldots, N\}$, and the set of edges, $\mathcal{E}_{\sigma(t)} \subseteq \mathcal{V} \times \mathcal{V}$. The edge $(i, j) \in \mathcal{E}_{\sigma(t)}$ shows that vehicle i and vehicle j are exchanging interactions, and a signal for topological switching $\sigma(t) : [0, +\infty) \to \mathcal{S}$, $\mathcal{S}$ denotes an index set that includes every likely communication topology. The graph $\mathcal{G}$ is defined by the adjacency matrix $\mathcal{A}_{\sigma(t)} = [a_{ij}(t)] \in \mathbb{R}^{(N+1)\times(N+1)}$ whose elements are such that $a_{ij}(t) = 1$ if the ith and the jth vehicles are adjacent vehicles of the graph $\mathcal{G}$; otherwise, $a_{ij}(t) = 0$. The Laplacian matrix is a time-varying matrix denoted $L_{\sigma(t)} = [l_{ij}(t)] \in \mathbb{R}^{(N+1)\times(N+1)}$, described as $l_{ii}(t) = \sum_{j=0, j\neq i}^{N} a_{ij}(t)$ and $l_{ij}(t) = -a_{ij}(t)$ for $i \neq j$. The graph Laplacian matrix $L_{\sigma(t)}$ in this situation has the following structure:

$$L_{\sigma(t)} = \begin{bmatrix} 0 & 0_{1\times N} \\ L_{1\sigma(t)} & L_{2\sigma(t)} \end{bmatrix}, \tag{2.1}$$

where $L_{1\sigma(t)} \in \mathbb{R}^{N\times 1}$ and $L_{2\sigma(t)} \in \mathbb{R}^{N\times N}$.

In addition, this necessitates a restatement of the topology-dependent average dwell-time (TDADT) formulation, as formally introduced. τ_{as} for the graph-theoretic switching signal $\sigma(t)$ is defined as long as $N_0^{\mathcal{S}}$ and τ_{as} are positive constants such that

$$N_\sigma^{\mathcal{S}}(t,T) \le N_0^{\mathcal{S}} + \frac{\mathcal{T}^s(t,T)}{\tau_{as}}, \qquad \forall T \ge t \ge 0, \tag{2.2}$$

where $\mathcal{T}^s(t,T)$ and $N_\sigma^{\mathcal{S}}(t,T)$ denote the running time and the cardinality of transitions for the sth topology across (t,T), respectively. The communication topology changes at a transition instant $t_1, t_2, \ldots$, and $t_{k+1} - t_k > 0$, $k \in \mathbb{N}^+$.

Assumption 1. For every admissible active topology $\mathcal{G}_s$, $s \in \mathcal{S}$, the leader vehicle is the root of a directed spanning tree; equivalently, the leader can reach every follower through a directed path in each active graph. Hence, each follower submatrix L_{2s} has the connectivity property required in Lemma 1. The term "joint connectivity" is reserved for the connectivity of a union of several graphs over an interval and is not the weaker condition used in the subsequent stability proof.

Lemma 1. When $t \in [t_k^i, t_{k+1}^i)$, it is feasible to define a component-wise positive definite vector

$$\mu_{\sigma(t)} = [\mu_1^{\sigma(t)}, \mu_2^{\sigma(t)}, \cdots, \mu_N^{\sigma(t)}]^T \in \mathbb{R}^N,$$

thereby ensuring

$$L_{2\sigma(t)}^T \mu_{\sigma(t)} = 1_N,$$

and

$$\Sigma_{\sigma(t)} L_{2\sigma(t)} + L_{2\sigma(t)}^T \Sigma_{\sigma(t)} > 0, \tag{2.3}$$

wherein

$$\Sigma_{\sigma(t)} = \mathrm{diag}\{\mu_1^{\sigma(t)}, \ldots, \mu_N^{\sigma(t)}\}.$$

2.2. Dynamics model of vehicular platoon systems

The considered vehicle platoon consists of multiple passenger vehicles. Each vehicle is equipped with an internal combustion engine powertrain, a five-speed automatic transmission, and a hydraulic retarder. This work primarily addresses the longitudinal dynamic characteristics of the vehicle system, which include non-affine elements like the powerplant, gearbox, and tire–road kinematic discrepancy.

The mathematical model of longitudinal dynamics is

$$\begin{cases} m\dot{v} = -mgf - \mathrm{sign}(v + v_{wd}) C_A (v + v_{wd})^2 - mg\sin(\varphi) + (T_d - T_b)/r_w, \\ T_{es} = MAP(\omega_e, \alpha_{thr}), \\ \tau_e \dot{T}_e + T_e = T_{es}/(\tau_e s + 1), \\ T_e = C_{TC}\omega_e^2 + J_e \dot{\omega}_e, \\ T_d = \eta_T i_g i_0 K_{TC} C_{TC} \omega_e^2, \\ \tau_d \dot{T}_b + T_b = K_b P_{brk}. \end{cases} \tag{2.4}$$

To address the dominant nonlinear phenomena, such as powertrains' static nonlinearity, non–continuous gear transitions, and quadratic drag forces, an inverse dynamic representation is implemented per nodal unit. Therefore, the vehicle model can be cast articulated through

$$\dot{x}_i(t) = Ax_i(t) + Bu_i(t), \qquad i \in \{1, \dots, N\}. \tag{2.5}$$

This governing equation for the leading agent is characterized by

$$\dot{x}_0(t) = Ax_0(t). \tag{2.6}$$

Remark 1. The primary objective of platoon control is twofold: To emulate the leader's velocity and to enforce a prescribed inter vehicle distance between adjacent followers. The reference state for a given node i is accordingly defined as

$$\begin{cases} v_i = v_0, \\ p_i = p_{i-1} - d_{i,i-1}, \end{cases} \tag{2.7}$$

where the desired distance between two consecutive vehicles is $d_{i,i-1}$. There is a more concise method to represent the relationship in equation

$$x_i = x_{i-1} - D_{i,i-1}, \tag{2.8}$$

wherein the state vector $x_i = [p_i \ v_i \ a_i]^T$ comprises positional, velocity, and acceleration states, while $D_{i,i-1} = [d_{i,i-1} \ 0 \ 0]^T$ defines the spacing vector. Equations (2.4)–(2.6) and Remark 1 describe two modeling levels. Equation (2.4) is the general nonlinear longitudinal vehicle model, while Eq (2.5) is the outer-loop representation obtained after inverse–dynamic compensation. For the theoretical development, x_i may contain position, velocity, and acceleration. In the numerical example, the inner inverse–dynamic loop is assumed to compensate the acceleration/powertrain dynamics, and the outer-loop state is therefore reduced to $x_i = [p_i \ v_i]^T$. Thus, the simulation is a reduced-order instantiation of Eq (2.5), not a different plant model.

The trajectory discrepancy for vehicle i with regard to the platoon leader is quantified by $\epsilon_i(t) = x_i(t) - x_0(t) - D_{i,0}$.

2.3. Intermittent communication model

The intermittent communication can cause packet transmission failures and hence can be regarded as a factor causing packet dropouts, especially in cyber-physical systems. In our study, we take into account potential disconnections in the communication channel among vehicles; attackers use virtual channel attacks to block communication information transmission in a wireless network.

This part examines the leader–follower synchronization in networked systems of linear agents characterized by switching communication topologies and vulnerability to intermittent communication. On each time interval $[t_h, t_{h+1})$, contemplate an unbounded progression of non-vanishing, adjacent, and uniformly bounded subintervals $[t_h^0, t_h^1), \cdots, [t_h^j, t_h^{j+1}), \cdots, [t_h^{j_h-1}, t_h^{j_h})$, where j_h is a positive integer. Define two sets of time intervals as:

$$\mathcal{A}_C = \underset{N}{\cup}[t_h^1, t_{h+1}) \cup [t_0, t_1), \tag{2.9}$$

$$\mathcal{A}_I = \underset{N}{\cup}[t_h, t_h^1), \tag{2.10}$$

where $t \in \mathcal{A}_C$ represents the time when communication is maintained, and $t \in \mathcal{A}_I$ represents the time when the system is under intermittent communication.

3. Collaborative resilience-oriented control synthesis and stability guarantees

For the i-th follower agent, define the reconstruction of the state vector, which is mathematically given by $\hat{x}_i(t) = e^{A(t-t_k^i)}x_i(t_k^i)$, $\forall t \in [t_k^i, t_{k+1}^i)$. Such measurement error $e_i(t)$ is captured by

$$e_i(t) = \hat{x}_i(t) - x_i(t), \quad i = 1, \cdots, N. \tag{3.1}$$

Each connected vehicle's control scheme is captured in

$$u_i(t) = \begin{cases} Kp_i^{\sigma(t)}, & \text{if } t \in \mathcal{A}_C, \\ 0, & \text{if } t \in \mathcal{A}_I, \end{cases} \tag{3.2}$$

wherein $K \in \mathbb{R}^{m\times n}$ constitutes the feedback compensation parameter matrix subject to synthesis; simultaneously, $p_i^{\sigma(t)}(t) = \sum_{j=1}^{N} a_{ij}^{\sigma(t)}(\hat{x}_i(t) - \hat{x}_j(t) - D_{i,j}) + a_{i0}^{\sigma(t)}(\hat{x}_i(t) - \hat{x}_0(t) - D_{i,0})$. Since the leader is an independent system, $\hat{x}_0(t) = x_0(t)$.

The trigger condition governing each follower is described by

$$f_i^{\sigma(t)}(t) = \|e_i(t)\| - g\left\|\sum_{j=1}^{N} a_{ij}^{\sigma(t)}(\hat{x}_i(t) - \hat{x}_j(t) - D_{i,j}) + a_{i0}^{\sigma(t)}(\hat{x}_i(t) - x_0(t) - D_{i,0})\right\|, \tag{3.3}$$

where g is a positive design parameter subject to the subsequent design.

The chronology of triggering connected vehicle t_k^i for each follower is given by

$$t_k^i = \begin{cases} t_h^j, & \text{if } \mathcal{G}_{\sigma(t)} \text{ switches}, \\ \inf\{t > t_{k-1}^i : f_i^{\sigma(t)}(t) > 0\}, & \text{alternatively}. \end{cases} \tag{3.4}$$

Theorem 1. Suppose that the matrices $Q > 0$ and R exist. Under the event-triggered controller in Eq (3.2), leader–follower consensus is guaranteed if the following conditions are satisfied.
(1) Determine the solution of the following LMIs

$$\begin{bmatrix} \aleph_{\sigma(t)} & \sum_{\sigma(t)} L_{2\sigma(t)} \otimes BR & 0 & L_{2\sigma(t)}^{\top} \otimes Q \\ * & -I_N \otimes Q & L_{2\sigma(t)}^{\top} \otimes Q & 0 \\ * & * & -\frac{1}{2N} I_{N\times n} & 0 \\ * & * & * & -\frac{1}{2N} I_{N\times n} \end{bmatrix} < 0, \tag{3.5}$$

and

$$AQ + QA^{\top} - \delta Q < 0, \tag{3.6}$$

where $\aleph_{\sigma(t)} = \Sigma_{\sigma(t)} \otimes AQ + \Sigma_{\sigma(t)} \otimes QA^{\top} + \Sigma_{\sigma(t)} L_{2\sigma(t)} \otimes BR + L_{2\sigma(t)}^{\top} \Sigma_{\sigma(t)} \otimes R^{\top} B^{\top} + \lambda_{\sigma(t)}(\Sigma_{\sigma(t)} \otimes Q)$, $\lambda_{\sigma(t)} > 0, \delta > 0$. We obtain the solution $Q > 0$.

(2) The gain matrix $K = RQ^{-1}$.
(3) The following conditions hold:

$$\sum_{s\in S}\left(\lambda_s - \frac{\ln \eta_s}{\tau_{as}}\right)T^s(t_0,t_1) - \ln\frac{d_0}{c_0} > 0, \tag{3.7}$$

$$\sum_{s\in S}\left(\lambda_s - \frac{\ln \eta_s}{\tau_{as}}\right)T^s(t_h^1,t_{h+1}) - \ln\frac{d_0}{c_0} > \delta(t_h^1 - t_h), \tag{3.8}$$

$$0 < g < \sqrt{\frac{1}{\lambda_{\max}(Q^{-1})}}, \tag{3.9}$$

where $\eta_s > (\lambda_{\max}(\Sigma_s)/\min_{s\in S}\{\lambda_{\min}(\Sigma_s)\})$, and c_0 and d_0 are given later, the collective of connected vehicle in Eqs (2.5) and (2.6) guarantees convergence to a leader–follower configuration. The synthesis is sequential rather than a simultaneous optimization: First solve the LMIs in Eqs (3.5) and (3.6) for Q and R and compute $K = RQ^{-1}$; then select g to satisfy the admissible bound in Eq (3.9). Therefore, the term "concurrent co-design" is not used here.

Proof. Let $\epsilon(t)$ as well as $e(t)$ represent the columnar arrays composed of $\epsilon_i(t)$ as well as $e_i(t)$, correspondingly. The tracking error system admits the representation

$$\dot{\epsilon}(t) = \begin{cases}(I_N\otimes A + L_{2\sigma(t)}\otimes BK)\epsilon(t) + (L_{2\sigma(t)}\otimes BK)e(t), & \text{if } t\in\mathcal{A}_C,\\ (I_N\otimes A)\epsilon(t), & \text{if } t\in\mathcal{A}_I.\end{cases} \tag{3.10}$$

We consider the following piecewise Lyapunov function

$$V_{\sigma(t)}(t) = \begin{cases}\epsilon^T(t)(\Sigma_{\sigma(t)}\otimes\bar{Q})\epsilon(t), & \text{if } t\in\mathcal{A}_C,\\ \epsilon^T(t)(I_N\otimes\bar{Q})\epsilon(t), & \text{if } t\in\mathcal{A}_I,\end{cases} \tag{3.11}$$

where $Q = \bar{Q}^{-1}$, and $\Sigma_{\sigma(t)}$ is defined in Lemma 1. Let $c_s = \lambda_{\min}(\Sigma_s)$, $c_0 = \min_{s\in S}\{c_s\}$, $\bar{c} = c_0\lambda_{\min}(\bar{Q})$, $d_s = \lambda_{\max}(\Sigma_s)$, $d_0 = \max_{s\in S}\{d_s\}$, $\bar{d} = d_0\lambda_{\max}(\bar{Q})$, and $\eta_s > (d_s/c_0)$. From Eq (3.11), we have

$$\begin{aligned}\bar{c}\|\epsilon(t)\|^2 &\le c_0\epsilon^T(t)(I_N\otimes\bar{Q})\epsilon(t) \le c_s\epsilon^T(t)(I_N\otimes\bar{Q})\epsilon(t) \le V_s(t)\\ &\le d_s\epsilon^T(t)(I_N\otimes\bar{Q})\epsilon(t) \le d_0\epsilon^T(t)(I_N\otimes\bar{Q})\epsilon(t) \le \bar{d}\|\epsilon(t)\|^2.\end{aligned} \tag{3.12}$$

Next, we will analyze $V_{\sigma(t)}(t)$ in three parts.
(1) When $t\in[t_h^1, t_{h+1})$, define $\sigma(t) = s$, $s\in S$. According to Eq (3.12), we have

$$V_{s1}(t) \le d_{s1}\epsilon^T(t)(I_N\otimes\bar{Q})\epsilon(t) \le \eta_{s1}V_{s2}(t), \tag{3.13}$$

where $s1, s2\in S$.

The evolution of the Lyapunov function candidate $V_s(t)$, when evaluated along the trajectories of the error dynamics in Eq (3.10), yields

$$\begin{aligned}\dot{V}_s(t) &= 2\epsilon^T(t)(\Sigma_s\otimes\bar{Q})[(I_N\otimes A)\epsilon(t) + (L_{2s}\otimes BK)\epsilon(t) + (L_{2s}\otimes BK)e(t)]\\ &= 2\epsilon^T(t)(\Sigma_s\otimes\bar{Q}A)\epsilon(t) + 2\epsilon^T(t)(\Sigma_sL_{2s}\otimes\bar{Q}BK)\epsilon(t) + 2\epsilon^T(t)(\Sigma_sL_{2s}\otimes\bar{Q}BK)e(t)\\ &\le \xi^T(t)\Phi_{1s}\xi(t) - \lambda_s\epsilon^T(t)(\Sigma_s\otimes\bar{Q})\epsilon(t) + \lambda_{\max}(\bar{Q})e^T(t)e(t),\end{aligned} \tag{3.14}$$

where

$$\Phi_{1s} = \begin{bmatrix} \aleph_{1s} & \Sigma_s L_{2s} \otimes \bar{Q}BK \\ * & -I_N \otimes \bar{Q} \end{bmatrix}, \quad \xi^T(t) = \begin{bmatrix} \epsilon^T(t) & e^T(t) \end{bmatrix},$$

$$\aleph_{1s} = \Sigma_s \otimes \bar{Q}A + \Sigma_s \otimes A^T\bar{Q} + \Sigma_s L_{2s} \otimes \bar{Q}BK + L_{2s}^T\Sigma_s \otimes K^T B^T\bar{Q} + \lambda_s(\Sigma_s \otimes \bar{Q}).$$

According to the driving condition in Eq (3.3), we have

$$\begin{aligned} \|e_i(t)\| &\le g \left\| \sum_{j=1}^{N} a_{ij}^s(\hat{x}_i(t) - \hat{x}_j(t) - D_{i,j}) + a_{i0}^s(\hat{x}_i(t) - x_0(t) - D_{i,0}) \right\| \\ &= g \left\| \sum_{j=1}^{N} a_{ij}^s(e_i(t) - e_j(t)) + a_{i0}^s e_i(t) + \sum_{j=1}^{N} a_{ij}^s(\epsilon_i(t) - \epsilon_j(t)) + a_{i0}^s\epsilon_i(t) \right\| \\ &\le g \left\| (L_{2s} \otimes I_n)e(t) + (L_{2s} \otimes I_n)\epsilon(t) \right\|. \end{aligned} \tag{3.15}$$

Therefore, we have

$$\sum_{i=1}^{N} \|e_i(t)\|^2 \le 2Ng^2 \left(\|(L_{2s} \otimes I_n)e(t)\|^2 + \|(L_{2s} \otimes I_n)\epsilon(t)\|^2 \right). \tag{3.16}$$

According to Eq (3.16), we have

$$\|e(t)\|^2 \le \xi^T(t) \begin{bmatrix} 2Ng^2(L_{2s}^T L_{2s} \otimes I_n) & 0 \\ 0 & 2Ng^2(L_{2s}^T L_{2s} \otimes I_n) \end{bmatrix} \xi(t). \tag{3.17}$$

According to $0 < g^2 < \frac{1}{\lambda_{\max}\bar{Q}}$, from Eqs (3.14) and (3.17), we have

$$\dot{V}_s(t) \le \xi^T(t)\Phi_{2s}\xi(t) - \lambda_s\epsilon^T(t)(\Sigma_s \otimes \bar{Q})\epsilon(t), \tag{3.18}$$

where

$$\Phi_{2s} = \begin{bmatrix} \aleph_{2s} & \Sigma_s L_{2s} \otimes \bar{Q}BK \\ * & -I_N \otimes \bar{Q} + 2N(L_{2s}^T L_{2s} \otimes I_n) \end{bmatrix},$$

$$\aleph_{2s} = \Sigma_s \otimes \bar{Q}A + \Sigma_s \otimes A^T\bar{Q} + \Sigma_s L_{2s} \otimes \bar{Q}BK + L_{2s}^T\Sigma_s \otimes K^T B^T\bar{Q} + \lambda_s(\Sigma_s \otimes \bar{Q}) + 2N(L_{2s}^T L_{2s} \otimes I_n).$$

Multiplying Φ_{2s} on both sides by $\mathrm{diag}\{I_N \otimes Q, I_N \otimes Q\}$ yields Φ_{3s}. By the Schur complement lemma, Eq (3.5) can be expressed as

$$\Phi_{3s} = \begin{bmatrix} \aleph_{3s} & \Sigma_s L_{2s} \otimes BR \\ * & -I_N \otimes Q + 2N(L_{2s}^T L_{2s} \otimes QQ) \end{bmatrix} < 0,$$

where $\aleph_{3s} = \Sigma_s \otimes AQ + \Sigma_s \otimes QA^T + \Sigma_s L_{2s} \otimes BR + L_{2s}^T\Sigma_s \otimes R^T B^T + \lambda_s(\Sigma_s \otimes Q) + 2N(L_{2s}^T L_{2s} \otimes QQ)$.

Therefore $\Phi_{2s} < 0$, and from Eq (3.18), we have

$$\dot{V}_s(t) \le -\lambda_s V_s(t). \tag{3.19}$$

According to the analysis above, when $t \in [t_h^1, t_h^{j_h}]$, from Eqs (3.13) and (3.19), we have

$$V_{\sigma(t_h^{j_h-1})}(t_h^{j_h-}) \leq \prod_{j=1}^{j_h-1} \eta_{\sigma(t_h^j)} \exp\left\{-\sum_{j=1}^{j_h-1} \lambda_{\sigma(t_h^j)}(t_h^{j+1} - t_h^j)\right\} V_{\sigma(t_h^1)}(t_h^1). \tag{3.20}$$

When $t \in [t_0, t_1)$, the communication network switches among finite directed graphs, and we have

$$V_{\sigma(t_0^{j_0-1})}(t_1^-) \leq \prod_{j=0}^{j_0-1} \eta_{\sigma(t_0^j)} \exp\left\{-\sum_{j=0}^{j_0-1} \lambda_{\sigma(t_0^j)}(t_0^{j+1} - t_0^j)\right\} V_{\sigma(t_0)}(t_0). \tag{3.21}$$

(2) When $t \in [t_h, t_h^1)$, the system is affected by cyber attacks. From Eqs (3.10) and (3.11), note that

$$\dot{V}_{\sigma(t)}(t) = \epsilon^T(t)[I_N \otimes (A^T\bar{Q} + \bar{Q}A)]\epsilon(t) \leq \delta V_{\sigma(t)}(t). \tag{3.22}$$

Therefore, for $t \in [t_h, t_h^1)$, from Eq (3.22), we have

$$V_{\sigma(t_h)}(t_h^{1-}) \leq \exp\left\{\delta(t_h^{1-} - t_h)\right\} V_{\sigma(t_h)}(t_h). \tag{3.23}$$

From Eq (3.12), we have

$$V_{\sigma(t_{h+1})}(t_{h+1}) \leq \frac{d_0}{c_0} V_{\sigma(t_h^{j_h-1})}(t_h^{j_h-}). \tag{3.24}$$

(3) When $t \in [t_h, t_{h+1}]$, from Eqs (3.20), (3.23), and (3.24), we have

$$V_{\sigma(t_{h+1})}(t_{h+1}) \leq \exp\left\{\ln\frac{d_0}{c_0} + \delta(t_h^1 - t_h) + \sum_{j=1}^{j_h-1} \ln\eta_{\sigma(t_h^j)} - \sum_{j=1}^{j_h-1} \lambda_{\sigma(t_h^j)}(t_h^{j+1} - t_h^j)\right\} V_{\sigma(t_h)}(t_h). \tag{3.25}$$

Let $\kappa_0 = \exp\left\{\sum_{s\in S} N_0^s \ln\eta_s\right\}$, $\varphi_h = \sum_{s\in S}\left(\lambda_s - \frac{\ln\eta_s}{\tau_{as}}\right) T^s(t_h^1, t_{h+1}) - \ln\frac{d_0}{c_0} - \delta(t_h^1 - t_h)$, $\varphi_0 = \sum_{s\in S}\left(\lambda_s - \frac{\ln\eta_s}{\tau_{as}}\right) T^s(t_0, t_1) - \ln\frac{d_0}{c_0}$. According to the analysis above, for $t \in [t_0, t_{h+1}]$, from Eqs (3.21) and (3.25), we have

$$V_{\sigma(t_{h+1})}(t_{h+1}) \leq \kappa_0 \exp\left\{-\sum_{h=1}^{h} \varphi_h - \varphi_0\right\} V_{\sigma(t_0)}(t_0). \tag{3.26}$$

As a terminal assertion, for all $t \geq 0$, the existence of a constant is guaranteed $c \geq 0$. We consider a compact set wherein all trajectories converge $t_c \leq t \leq t_{c+1}$. Let $\mu = \max_{h\in\mathbb{N}}\{t_{c+1} - t_c\}$ and $\underline{\varphi} = \min_{c\in\mathbb{N}}\{\varphi_c\}$, we can derive

$$V_{\sigma(t_c)}(t) \leq \kappa_0 \exp\{\delta\mu\} \exp\left\{-c\underline{\varphi}\right\} V_{\sigma(t_0)}(t_0) \leq \kappa \exp\{-\zeta(t - t_0)\} V_{\sigma(t_0)}(t_0), \tag{3.27}$$

where $\kappa = \kappa_0 \exp\left\{\delta\mu + \underline{\varphi}\right\}$ and $\zeta = \underline{\varphi}/\mu$.

From Eq (3.12), we have

$$\|\epsilon(t)\|^2 \leq \frac{\kappa\bar{d}}{\bar{c}} e^{-\zeta(t-t_0)} \|\epsilon(t_0)\|^2. \tag{3.28}$$

This result establishes that the collective of connected vehicle is demonstrably capable of achieving coordinated tracking with the designated leader. □

For clarity, define the stacked interaction vector $p^{\sigma(t)}(t) = \text{col}\{p_1^{\sigma(t)}(t), \ldots, p_N^{\sigma(t)}(t)\}$.

Theorem 2. The collectives of connected vehicles in Eq (2.5) and (2.6) preclude the occurrence of Zeno phenomena.

Proof. When the triggering condition in Eq (3.3) causes any two consecutive triggers, using Eq (3.1) and the definition of $p_i^{\sigma(t)}(t)$, we have

$$\|\dot{e}(t)\| \leq \|I_N \otimes A\| \, \|e(t)\| + \|I_N \otimes BK\| \left\|p^{\sigma(t)}(t)\right\|,$$

let

$$\|I_N \otimes A\| = \alpha_1 \quad \text{and} \quad \|I_N \otimes BK\| = \alpha_2.$$

Here, α_1 and α_2 are finite induced-norm bounds determined by the closed-loop system matrices. They convert the vector differential inequality into a scalar growth bound for the measurement error. Then

$$\|\dot{e}(t)\| \leq \alpha_1 \, \|e(t)\| + \alpha_2 \left\|p^{\sigma(t)}(t)\right\|.$$

From the definition of $p_i^{\sigma(t)}(t)$, we have

$$\|p_i^{\sigma(t)}(t)\| \leq \beta(\|e(t)\| + \|\epsilon(t)\|.$$

By Theorem 1, the tracking error is exponentially convergent and hence bounded. Together with the bounded graph weights and the bounded measurement error between two events, this implies that a finite constant $M > 0$ exists such that

$$\|p_i^{\sigma(t)}(t)\| \leq M.$$

Consequently,

$$\|\dot{e}(t)\| \leq \alpha_1 \, \|e(t)\| + \alpha_2 M.$$

Between two triggering instants, for $t \in [t_k^i, t_{k+1}^i)$, we obtain

$$\|e(t)\| \leq \frac{\alpha_2 M}{\alpha_1} \left(e^{\alpha_1 (t - t_k^i)} - 1\right).$$

According to the triggering condition in Eq (3.3), when no event is triggered, it holds that

$$\|e_i(t)\| < g\|p_i^{\sigma(t)}(t)\|.$$

Let $M_p > 0$ be a uniform upper bound of $\|p_i^{\sigma(t)}(t)\|$ over the admissible switching modes and the considered bounded trajectories. This constant is used only to upper-bound the triggering threshold. Hence, we have

$$\|e(t)\| < gM_p.$$

Starting from $e_i(t_k^i) = 0$, the comparison inequality above gives the fastest admissible growth envelope of the measurement error. To reach the triggering threshold, a strictly positive amount of time is therefore required. In particular, the interval from t_k^i to t_{k+1}^i satisfies

$$\frac{\alpha_2 M}{\alpha_1} \left(e^{\alpha_1 (t_{k+1}^i - t_k^i)} - 1\right) \geq gM_p,$$

which yields

$$t_{k+1}^i - t_k^i \geq \frac{1}{\alpha_1} \ln\left(1 + \frac{\alpha_1 g M_p}{\alpha_2 M}\right) > 0.$$

Therefore, the connected vehicle system does not exhibit Zeno behavior.

4. Simulation example

This segment presents a numerical simulation to corroborate the efficacy of the devised event-triggered methodology. The interconnection architecture is graphically represented in Figure 1, with the switching rule $G_a \to G_b \to \cdots \to G_d \to G_a \to \cdots$.

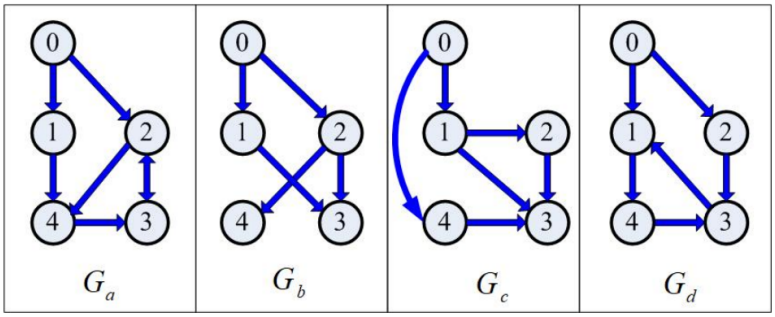


Figure 1. Topology switching signal.

Figure 1 illustrates the prescribed sequence among the four admissible topologies (e.g., $G_a \to G_b \to \cdots \to G_d \to G_a \ldots$) used in the numerical evaluation. Its switching times satisfy the topology-dependent average dwell-time assumptions used in the analysis. Consistent with the clarification following Remark 1, the general outer-loop model in Eq (2.5) is instantiated in the simulation with $n = 2$ and $m = 2$. The simulated state is the reduced-order longitudinal vector $x_i = [p_i \ v_i]^T$, while the omitted acceleration/powertrain dynamics are handled by the inverse-dynamic inner loop. Consequently, A, B, and K are all 2×2, consistent with the MATLAB/Simulink implementation. The coefficient matrices A and B are parameterized as

$$A = \begin{bmatrix} -1.175 & 0.9871 \\ -8.458 & -0.8776 \end{bmatrix}, \quad B = \begin{bmatrix} -0.194 & -0.03593 \\ -19.29 & -3.803 \end{bmatrix}.$$

The system is initialized with

$$\begin{aligned} x_0(0) &= [0, -0.5]^T, \\ x_1(0) &= [-3, -6.8]^T, \\ x_2(0) &= [0, -4.5]^T, \\ x_3(0) &= [1, 2]^T, \\ x_4(0) &= [-1, -2.8]^T. \end{aligned}$$

The system parameters are selected as $\lambda_1 = 1.45, \lambda_2 = 1.53, \lambda_3 = 1.62, \lambda_4 = 1.58, \delta = 2.5$, and $g = 0.75$. The controller is evaluated with a 0.01 s sampling period. In the sampled implementation, a 0.05 s hold-off is applied only to repeated threshold-induced events, together with a 0.01 numerical deadband and a 2 s maximum synchronization interval. A topology change or recovery from an intermittent–communication interval causes immediate synchronization and may therefore bypass the threshold hold-off. These sampled–data safeguards belong only to the engineering implementation. In contrast, Theorem 2 establishes a continuous-time positive lower bound on the inter event interval and is the analytical basis for Zeno exclusion.

Using Theorem 1, the matrix K can be obtained as follows:

$$K = \begin{bmatrix} 23.7923 & -0.1898 \\ -120.6890 & 1.0204 \end{bmatrix}.$$

The numerical simulation results (see Figures 1–5) corroborate the convergence and communication–efficiency trends predicted by the analysis. Specifically, the tracking errors converge to a neighborhood of the origin under intermittent communication, and the proposed controller handles the prescribed switching sequence. Figures 2–5 show fast error recovery after each communication interruption, accurate reduced-order position/velocity tracking, and sparse communication updates. The Zeno-free property itself follows from Theorem 2 rather than from the sampled simulation; the unprotected interval statistics reported below provide only a numerical consistency check at the 0.01 s sampling resolution.

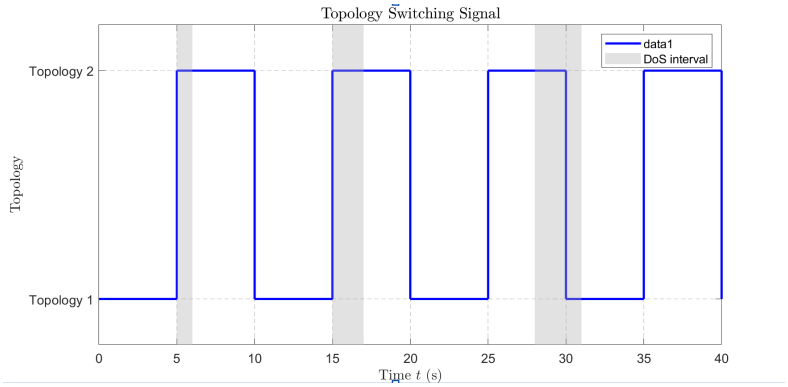


Figure 2. The structural reconfiguration sequence.

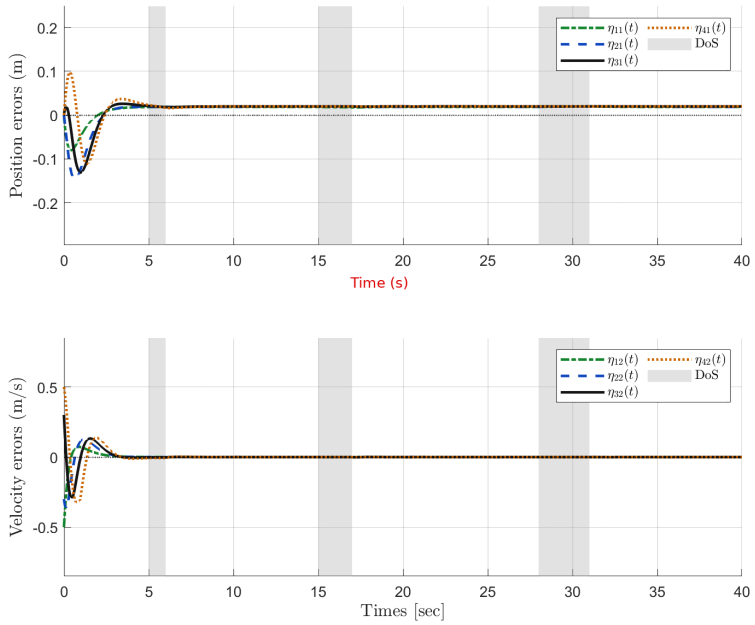


Figure 3. Tracking error under intermittent communication.

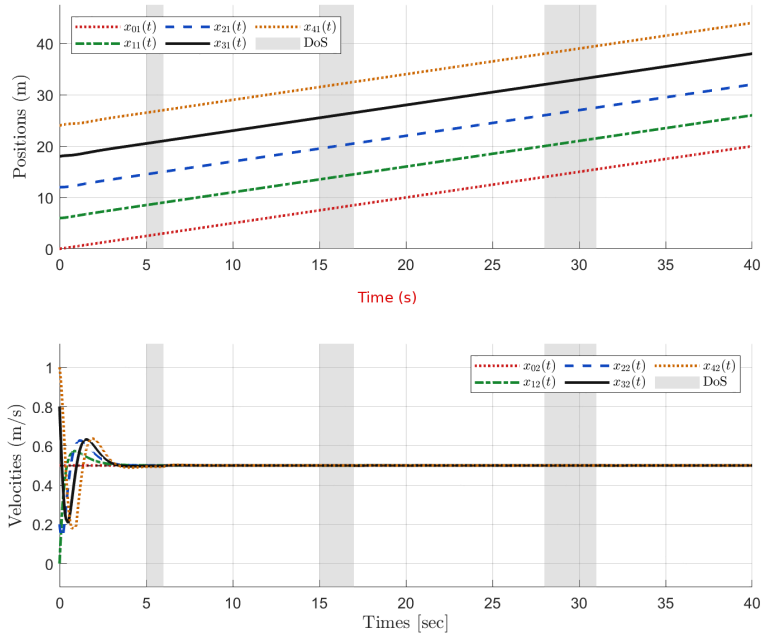


Figure 4. State trajectories under intermittent communication.

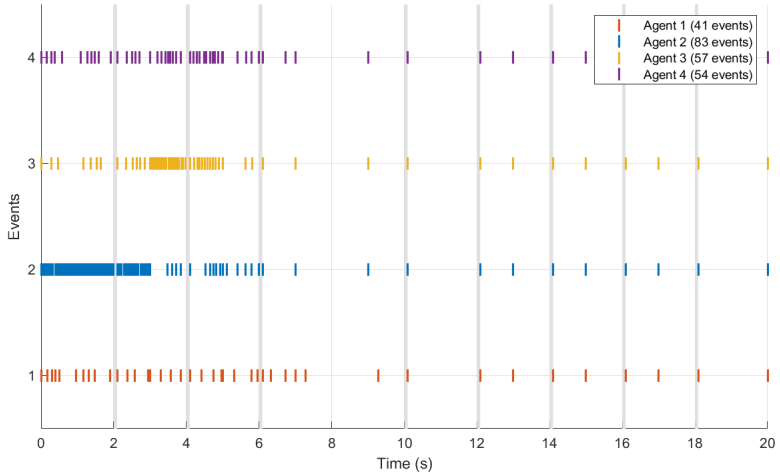


Figure 5. Triggering epochs with the engineering threshold hold-off for $i = 1, 2, 3, 4$.

4.1. Ablation comparisons

All ablations use the same initial conditions, intermittent–communication pattern, controller gain, solver settings, colors, and line widths. For clarity, one communication update is counted whenever one follower's binary trigger output equals one in a 0.01 s sample; the reported total is the sum over all four followers and all samples in $[0, 20]$ s. During a communication interruption, the binary trigger outputs are zero and no update is counted. The no-event-trigger baseline updates every follower at

every communication-available sample. The aggregate tracking error plotted in Figure 6 is

$$E(t_k) = \left(\sum_{i=1}^{4} \|x_i(t_k) - x_0(t_k)\|_2^2 \right)^{1/2},$$

and its reported root mean square (RMS) is the discrete full-horizon value

$$E_{\mathrm{RMS}} = \left(\frac{1}{M} \sum_{k=1}^{M} E^2(t_k) \right)^{1/2}, \qquad t_k \in [0, 20]\,\mathrm{s}.$$

As shown in Figure 6, the aggregate–error curves are close, whereas the number of transmissions increases from 235 to 7684 without triggering events. Thus, the proposed strategy reduces communication updates by 96.94%, while E_{RMS} changes from 1.25536 for the no-event-trigger baseline to 1.26407, a relative difference of approximately 0.69%. This comparison therefore supports a communication–efficiency advantage while maintaining comparable tracking accuracy, rather than a claim of uniformly smaller tracking error.

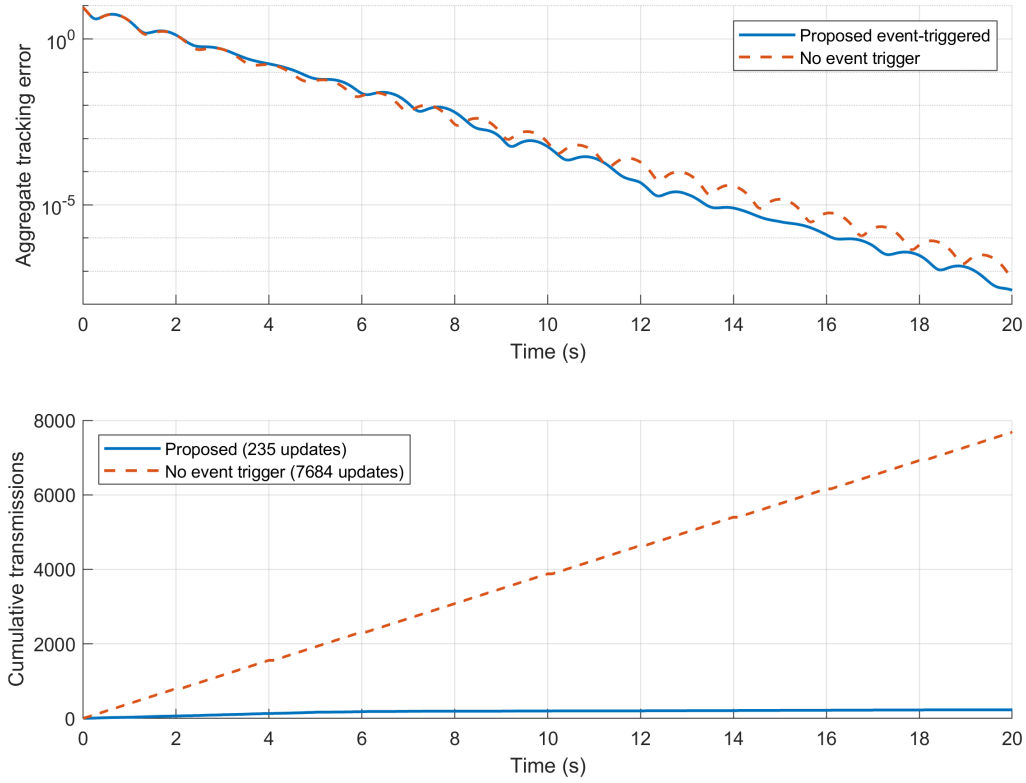


Figure 6. Comparison with no event triggering: Aggregate tracking performance and cumulative transmissions.

4.1.1. Sensitivity to the engineering hold-off

To separate the engineering hold-off from the analytical Zeno result, the switching–topology simulation is repeated with the threshold hold-off set to zero while all other settings are unchanged. Table 1 reports the intervals between consecutive events for each follower. The unprotected

implementation produces 434 events and $E_{\mathrm{RMS}} = 1.26241$, compared with 235 events and $E_{\mathrm{RMS}} = 1.26407$ with the hold-off. Its minimum observed interval is 0.01 s, equal to the sampling period. Therefore, this numerical result shows no event accumulation at the available resolution, but it is not an independent proof of Zeno exclusion.

Table 1. Event statistics without the 0.05 s threshold hold-off.

Follower	Events	Minimum (s)	Median (s)	Mean (s)
1	39	0.030	0.315	0.526
2	271	0.010	0.010	0.074
3	72	0.010	0.070	0.282
4	52	0.030	0.160	0.392

4.1.2. Comparison with all fixed topologies

The topology ablation is repeated by freezing each admissible graph G_a, G_b, G_c, and G_d over the complete simulation horizon. Figure 7 and Table 2 show that every case converges. The switching–topology RMS lies within 1.3% of the range obtained for the four fixed graphs. The fixed G_b and G_d cases have slightly smaller RMS values, whereas the switching case accommodates repeated structural reconfiguration without loss of convergence. Accordingly, this ablation supports topology adaptability and comparable performance, rather than uniform dominance over every fixed graph.

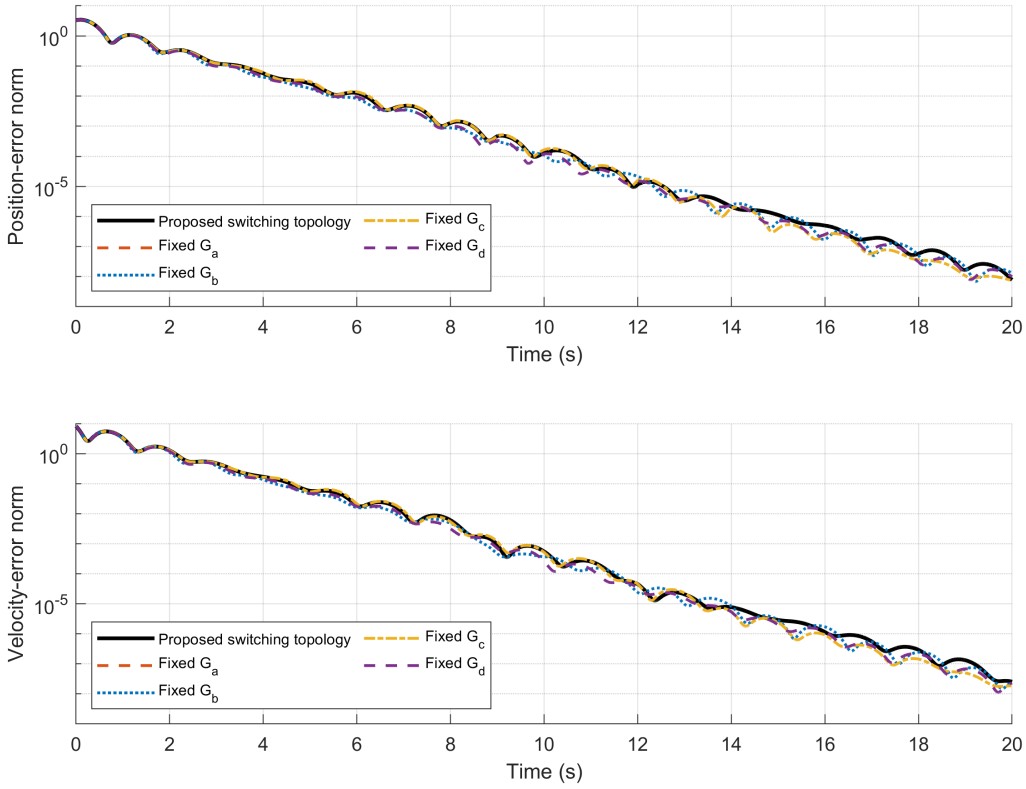


Figure 7. Switching topology compared with a fixed G_a, G_b, G_c, and G_d: Position and velocity error norms.

Table 2. Performance under switching and fixed topologies.

Topology	Events	E_{RMS}	IAE	Peak $E(t)$, $t \geq 5$ s
Switching	235	1.26407	8.071	0.06327
Fixed G_a	204	1.26415	8.086	0.06605
Fixed G_b	209	1.25084	7.769	0.04983
Fixed G_c	204	1.26415	8.086	0.06605
Fixed G_d	213	1.24844	7.774	0.05084

Note: E_{RMS} denotes the root-mean-square error, IAE denotes the integral absolute error, and Peak $E(t), t \geq 5$s represents the maximum value of the error after 5 seconds. Events is the total number of triggering events.

5. Conclusions

This paper investigates the coordinated tracking problem for a class of vehicle platoons within the connected vehicle system framework, with a focus on the challenges induced by switching communication topologies and intermittent communication. An innovative control strategy based on an event-triggered mechanism has been constructed to effectively address the complex control problem under limited communication resources and simultaneous cyber attacks.

The principal innovations of this study are delineated below.

1. **A longitudinal vehicle dynamic model with strong nonlinearities was established, and a decentralized event-driven control scheme was formulated.** This controller utilizes the estimated states of neighboring vehicles for feedback control during communication-normal intervals ($\mathcal{A}_C$) and adopts a zero-control-input strategy during intermittent communication intervals ($\mathcal{A}_I$), thereby enhancing the system's resilience against disruptions.

2. **A stability analysis framework for the closed-loop system under topology-dependent average dwell time constraints was proposed.** By constructing a switching Lyapunov function dependent on the communication topology and jointly considering the constraints on the temporal characteristics of malicious cyber engagements, it was rigorously proven that the tracking error system is exponentially stable. This guarantees that the system achieves leader–follower consensus.

3. **Analytical verification shows that the introduced event-triggered scheme avoids Zeno behavior.** A strictly positive lower bound governing inter triggering durations was theoretically guaranteed, ensuring the practical implementability of the control strategy.

4. **An LMI-based controller-gain synthesis, together with an explicit admissible range for the triggering parameter, was provided.** The controller gain is obtained from the feasible LMIs, after which the triggering parameter is selected to satisfy the condition in Eq (3.9). This formulation avoids implying a simultaneous optimization that is not required by Theorem 1.

The theoretical analysis establishes stability and Zeno exclusion, while the numerical results show a substantial reduction in communication updates with comparable tracking performance. The fixed-topology comparisons further indicate robustness and adaptability to repeated topology

reconfiguration; they do not imply uniform performance superiority over every fixed-topology case. Future research will prioritize extending this framework to more complex network attack scenarios (e.g., deception attacks), systems with time-varying delays, and more general nonlinear multi-agent systems.

Use of AI tools declaration

The authors declare they have not used artificial intelligence (AI) tools in the creation of this article.

Conflict of interest

The authors declare there is no conflict of interest.

Acknowledgments

This work was partially supported by the Heilongjiang Provincial Natural Science Foundation of China (No. PL2025F035), and the Fundamental Research Funds for the provincial universities of Heilongjiang Province (No. 2025-KYYWF-ZR0397).

Author contributions

Xin Wen: Conceptualization, Methodology, Formal analysis, Writing—original draft. Tingting Yu: Methodology, Writing—review and editing, Supervision, Funding acquisition. Ruibing Li: Investigation, Formal analysis, Software. All authors have read and approved the final manuscript.

References

1. Y. Liu, K. M. Passino, Stable social foraging swarms in a noisy environment, *IEEE Trans. Autom. Control*, **49** (2004), 30–44. https://doi.org/10.1109/TAC.2003.821416
2. H. Su, X. Wang, Z. Lin, Flocking of multi-agents with a virtual leader, *IEEE Trans. Autom. Control*, **54** (2009), 293–307. https://doi.org/10.1109/TAC.2008.2010897
3. J. Qin, C. Yu, Cluster consensus control of generic linear multi-agent systems under directed topology with acyclic partition, *Automatica*, **49** (2013), 2898–2905. https://doi.org/10.1016/j.automatica.2013.06.017
4. F. Cucker, S. Smale, Emergent behavior in flocks, *IEEE Trans. Autom. Control*, **52** (2007), 852–862. https://doi.org/10.1109/TAC.2007.895842
5. P. Yang, R. A. Freeman, K. M. Lynch, Multi-agent coordination by decentralized estimation and control, *IEEE Trans. Autom. Control*, **53** (2008), 2480–2496. https://doi.org/10.1109/TAC.2008.2006925
6. W. Zhang, J. Hu, Optimal multi-agent coordination under tree formation constraints, *IEEE Trans. Autom. Control*, **53** (2008), 692–705. https://doi.org/10.1109/TAC.2008.919855

7. Y. Hatano, M. Mesbahi, Agreement over random networks, *IEEE Trans. Autom. Control*, **50** (2005), 1867–1872. https://doi.org/10.1109/TAC.2005.858670

8. M. M. Gulzar, S. T. H. Rizvi, M. Y. Javed, U. Munir, H. Asif, Multi-agent cooperative control consensus: A comparative review, *Electronics*, **7** (2018), 22. https://doi.org/10.3390/electronics7020022

9. A. Coppola, D. G. Lui, A. Petrillo, S. Santini, Distributed fixed-time leader-tracking control for heterogeneous uncertain autonomous connected vehicles platoons, in *2021 29th Mediterranean Conference on Control and Automation (MED)*, PUGLIA, Italy, 2021, 554–559. https://doi.org/10.1109/MED51440.2021.9480345

10. S. Parkinson, P. Ward, K. Wilson, J. Miller, Cyber threats facing autonomous and connected vehicles: Future challenges, *IEEE Trans. Intell. Transp. Syst.*, **18** (2017), 2898–2915. https://doi.org/10.1109/TITS.2017.2665968

11. Z. A. Biron, S. Dey, P. Pisu, Real-time detection and estimation of denial of service attack in connected vehicle systems, *IEEE Trans. Intell. Transp. Syst.*, **19** (2018), 3893–3902. https://doi.org/10.1109/TITS.2018.2791484

12. S. Feng, P. Tesi, Resilient control under denial-of-service: Robust design, *Automatica*, **79** (2017), 42–51. https://doi.org/10.1016/j.automatica.2017.01.031

13. B. Chen, D. W. C. Ho, W. A. Zhang, L. Yu, Distributed dimensionality reduction fusion estimation for cyber-physical systems under DoS attacks, *IEEE Trans. Syst., Man, Cybern. Syst.*, **49** (2017), 455–468. https://doi.org/10.1109/TSMC.2017.2697450

14. C. De Persis, P. Tesi, Input-to-state stabilizing control under denial-of-service, *IEEE Trans. Autom. Control*, **60** (2015), 2930–2944. https://doi.org/10.1109/TAC.2015.2416924

15. D. Zhang, Y. P. Shen, S. Q. Zhou, X. W. Dong, L. Yu, Distributed secure platoon control of connected vehicles subject to DoS attack: Theory and application, *IEEE Trans. Syst., Man, Cybern. Syst.*, **51** (2020), 7269–7278. https://doi.org/10.1109/TSMC.2020.2968606

16. S. Öncü, J. Ploeg, N. Van de Wouw, H. Nijmeijer, Cooperative adaptive cruise control: Network-aware analysis of string stability, *IEEE Trans. Intell. Transp. Syst.*, **15** (2014), 1527–1537. https://doi.org/10.1109/TITS.2014.2302816

17. F. Gao, X. Hu, S. E. Li, K. Li, Q. Sun, Distributed adaptive sliding mode control of vehicular platoon with uncertain interaction topology, *IEEE Trans. Ind. Electron.*, **65** (2018), 6352–6361. https://doi.org/10.1109/TIE.2017.2787574

18. W. Hu, C. Yang, T. Huang, W. Gui, A distributed dynamic event-triggered control approach to consensus of linear multiagent systems with directed networks, *IEEE Trans. Cybern.*, **50** (2018), 869–874. https://doi.org/10.1109/TCYB.2018.2868778

19. B. Cheng, Z. Li, Fully distributed event-triggered protocols for linear multiagent networks, *IEEE Trans. Autom. Control*, **64** (2018), 1655–1662. https://doi.org/10.1109/TAC.2018.2857723

20. D. Yang, W. Ren, X. Liu, W. Chen, Decentralized event-triggered consensus for linear multi-agent systems under general directed graphs, *Automatica*, **69** (2016), 242–249. https://doi.org/10.1016/j.automatica.2016.03.003

21. Y. Zhao, Y. Liu, H. Zhang, N. Zhao, Y. Shi, Funnel-based predefined-time output feedback fuzzy adaptive event-triggered platoon control for heterogeneous vehicles, *IEEE Internet Things J.*, **13** (2026), 39672–39682. https://doi.org/10.1109/JIOT.2026.3706788

22. C. Deng, M. Ye, L. Ding, D. Yue, S. Fan, Nash equilibrium seeking for high-order nonlinear MASs under event-triggered communication, *Automatica*, **187** (2026), 112849. https://doi.org/10.1016/j.automatica.2026.112849

23. S. Fan, H. Yan, W. Che, C. Deng, Cooperative resilient nonconvex optimization control for nonlinear MASs under DoS attacks, *Sci. China Inf. Sci.*, **69** (2026), 172207. https://doi.org/10.1007/s11432-025-4919-0

24. G. Zhang, Z. Li, J. Li, J. Huang, Robust event-triggered path following control for a rotor-assisted vehicle with output constraints: Theory and experiment, *IEEE Trans. Ind. Electron.*, **73** (2026), 10594–10604. https://doi.org/10.1109/TIE.2026.3656989

25. G. Wu, G. Chen, H. Zhang, C. Huang, Fully distributed event-triggered vehicular platooning with actuator uncertainties, *IEEE Trans. Veh. Technol.*, **70** (2021), 6601–6612. https://doi.org/10.1109/TVT.2021.3086824



AIMS Press

© 2026 the Author(s), licensee AIMS Press. This is an open access article distributed under the terms of the Creative Commons Attribution License (https://creativecommons.org/licenses/by/4.0)